Biomass Conversion and Biorefinery
https://doi.org/10.1007/s13399-023-03914-6

ORIGINAL ARTICLE

Biosorption of lead ions (Pb^{2+}) from water samples using dried *Lemna minor* biomass: experimental and density functional theory studies

Savaş Kaya[1] · Serap Çetinkaya[2] · Nida Shams Jalbani[3] · Ali Fazıl Yenidünya[2] · Nurşah Kütük[4] · Ergün Kasaka[5] · Mikhail M. Maslov[6]

Received: 17 November 2022 / Revised: 24 January 2023 / Accepted: 5 February 2023

Abstract
Lemna minor biomass, a novel source of biosorbent, was found to exhibit high adsorption potential over a wide range of concentrations of Pb^{2+}. The biosorbent was characterized by Fourier transform infrared (FTIR) spectrophotometry, scanning electron microscopy (SEM), energy-dispersive X-ray (EDX) analysis, X-ray powder diffraction (XRD), and thermogravimetric analysis (TGA). Biosorption experiments were carried out under the optimized parameters such as solution pH, biosorbent amount, equilibrium time, and temperature. During the sorption, it has been observed that the above 85% removal of Pb^{2+} ions was achieved at acidic pH (4.5–5.1). Moreover, the maximum sorption was achieved using the 150 mg L^{-1} biosorbent. Equilibrium experiments were validated by the Langmuir, Freundlich, and Dubinin–Radushkevich isotherm models. From the results, it has been noticed that the experimental data was best fitted to the Langmuir model (R^2, 0.986 and 969.18 mmol g^{-1}). Standard enthalpy ($\Delta H°$), free energy ($\Delta G°$), and entropy ($\Delta S°$) changes were calculated. Results showed that biosorption of Pb^{2+} was spontaneous and endothermic. The biosorption mechanism was analyzed through pseudo-first-order and pseudo-second-order kinetic models. The results demonstrated that the biosorption of Pb^{2+} followed the pseudo-second-order kinetic model. Adsorbate-adsorbent interactions were scrutinized by density functional theory (DFT).

Keywords *Lemna minor* biomass · Biosorption · Pb^{2+} ions · Equilibrium models · DFT study · Thermodynamic study

1 Introduction

Degradation of water quality by industrial pollutants has been seen as a major obstacle to sustainable development because it poses a serious threat to the globe. The main perpetrator of this challenge is the increase in population in parallel to global industrialization efforts. One of the concerns involves heavy metal pollutants such as copper, lead, chromium, cadmium, and mercury. Through the food chain, they have become detrimental agents to human health [1].

Lead is a common environmental toxic pollutant [2] as it can accumulate in the body at elevated concentrations and

✉ Savaş Kaya
savaskaya@cumhuriyet.edu.tr

Serap Çetinkaya
secetinkaya@cumhuriyet.edu.tr

Nida Shams Jalbani
nidajchemist.88@gmail.com

Ali Fazıl Yenidünya
afazil@cumhuriyet.edu.tr

Nurşah Kütük
nkutuk@cumhuriyet.edu.tr

Ergün Kasaka
ekasaka@cumhuriyet.edu.tr

Mikhail M. Maslov
mike.maslov@gmail.com

[1] Department of Pharmacy, Health Services Vocational School, Sivas Cumhuriyet University, 58140 Sivas, Turkey

[2] Department of Molecular Biology and Genetics, Science Faculty, Sivas Cumhuriyet University, 58140 Sivas, Turkey

[3] National Center of Excellence in Analytical Chemistry, University of Sindh, Jamshoro 76080, Pakistan

[4] Department of Chemical Engineering, Faculty of Engineering, Sivas Cumhuriyet University, Sivas, Turkey

[5] Yıldızeli Meslek Yüksekokulu, Sivas Cumhuriyet Üniversitesi, Yıldızeli, Sivas, Turkey

[6] Nanoengineering in Electronics, Spintronics and Photonics Institute, National Research Nuclear University "MEPhI", Kashirskoe Shosse, Moscow, Russia

Published online: 24 February 2023

cause anemia, infertility, hypertension, memory loss, miscarriage, kidney disorders, and mental retardation [3, 4]. According to USEPA guidelines [5], the safety limit of lead in drinking water is 15 μg L^{-1}.

Removal of heavy metals from aqueous solutions with biomass can be considered as an alternative process for industrial wastewater treatment. In this respect, aquatic plants stand to have a great potential for the removal of ionic pollutants from aqueous environments [6, 7]. Among the plants studied, floating macrophytes (macroalgae, duckweed, water hyacinth) offer better advantages as they grow faster and are readily harvested [7, 8].

Biosorption technology offers advantages such as low operation costs, regeneration potential, minimized disposal volumes, and high adsorption efficiency at very dilute concentrations. The use of dead, dried aquatic plants as a simple biosorbent material for the removal of metals from industrial waters has been increasing in recent years. This technology is based on the ability of biological materials to sequester heavy metals through metabolic activities or by purely physical–chemical removal pathways [9].

Selection of the most suitable aquatic plant species for metal removal includes several factors such as biomass yield, ease of growth, and harvesting [10]. The adsorption of heavy metals can be mainly attributed to proteins, carbohydrates, and phenolic compounds by virtue of their metal-binding carboxyl, hydroxyl, sulfate, phosphate, and amino groups. Adsorption through these functional groups often involves the exchange of hydrogen ions with metal ions [11–14]. Aquatic plants are organisms with high carbon content that are distributed all over the world. Among them is *Lemna minor* (duckweed) [15]. They have strong adsorption capacity for heavy metals, such as lead and cadmium, during their growth period [16–18]. This plant can double its mass in a few days under suitable growing conditions. It is usually found in shallow still-water bodies. Its interaction with sediments contributes to its rapid growth [19]. However, it is unknown whether biochar produced from *L. minor* still has effective adsorption capacity for heavy metals [20–23].

Current study explores the novel application of *Lemna minor* biosorbent for the removal of Pb^{2+} metal ions from water under the optimized adsorption parameters such as contact time, pH of solution, biomass amount, and initial Pb^{2+} concentration. Moreover, the SEM, EDX, FTIR, XRD, and TGA techniques were used to characterize the biosorbent and investigate possible mechanism of the biosorption reaction. Furthermore, the DFT modeling was also applied to the experimental findings.

2 Materials and methods

2.1 Preparation of adsorbent and metal solutions

L. minor was collected from Lake Hafik (Sivas, Turkey) and washed several times under tap water and then with deionized water. It was powdered after drying in an oven at 60 °C for 3 h [14].

Pb^{2+} stock solution, 1000 mg L^{-1}, was prepared from analytical grade lead nitrate ($Pb(NO_3)_2$; ≥ 99.0%, Sigma-Aldrich). Deionized water was used for all dilutions. Pb^{2+} concentrations were measured at 503 nm (UV–Vis spectrophotometer, T60, China).

2.2 Experimental procedure

2.2.1 Determination of pH and ion concentrations after adsorption

Initial Pb^{2+} solutions, 200 ppm and 10 mL, were prepared within a pH range from 1 to 5.5, using 0.1 mol L^{-1} HCl or NaOH. Onto these solutions, adsorbent (0.3 g, 0.05 g, 0.1 g, or 0.25 g) was added, and final sample was incubated for 24 h at 5, 25, or 40 °C. Final pH was measured, and the ion concentration was checked periodically during biosorption reaction.

2.2.2 Reusability (regeneration)

After adsorption, the solid phases were first regenerated in 20 mL of 0.1 mol L^{-1} HCl and then in 20 mL NaOH (0.1 mol L^{-1}) and ethyl alcohol (0.1 mol L^{-1}). Ion contents were read. The adsorbent was washed with distilled water before reuse.

2.2.3 PZC (the point of zero charge)

To determine the PZC values of the biosorbent, the pH of KNO_3 (0.1 mol L^{-1}) was adjusted within a pH range, from 1 to 12, using HCl or NaOH (0.1 mol L^{-1}). Fifty milligrams of biosorbent was added. Initial pH values were then plotted against ΔpH to obtain PZC [24]. Final pH values were read after 24 h.

2.3 Details of DFT calculations

All calculations were performed using the Perdew–Burke–Ernzerhof (GGA-PBE) exchange–correlation functional [25] and split valence polarization def2-SVP electronic basic set [26]. The dispersion corrections D3 proposed by Grimme et al. [27] were also included to take into account

the weak non-covalent interactions. So, the PBE-D3/def2-SVP level of theory was applied, and graphics processor-based TeraChem software [28–31] was used. Geometry optimization was carried out with the efficient geometric energy minimizer [32, 33].

3 Results and discussion

3.1 Characterization studies

3.1.1 FTIR analysis

Chemical structure of *L. minor* was investigated by FTIR spectroscopy (4000–400 cm^{-1}) before and after biosorption (Fig. 1). The main peaks seen indicated the following events: An N–H stretching at 3277 cm^{-1}, caused by amino acids [34, 35]; C-H stretching from lipids at 2922 cm^{-1}; O–H band at 1421 cm^{-1}, from phenolics; A C = O stretch from carboxylic acids at 1615 cm^{-1}; C-O stretching at 1319 cm^{-1}, and C–O–C and O–H vibrations of polysaccharides and hemicellulose at 1021 cm^{-1}; at 875 cm^{-1}, a Si–H bend; and the peaks with a wavenumber lower than 800 cm^{-1} were the fingerprint region containing the phosphate and sulfur functional groups [34–36]. These results indicated that functional groups such as carboxyl group, hydroxyl group, polysaccharide, and cellulose in *L. minor* participated in biosorption. As expected, the intensity of the peaks changed after biosorption [37].

3.1.2 XRD characterization

The peaks in 14.9°, 24.4°, 29.4°, and 36.1° specified the crystal structure of the *L. minor* (Fig. 2) [38]. There were mixed crystal and amorphous organic compounds in the structure. The peak in $2\theta = 24.4°$ was attributed to the cellulose [39]. After biosorption, a significant decrease occurred in the density of the peak at $2\theta = 29.5°$. This peak

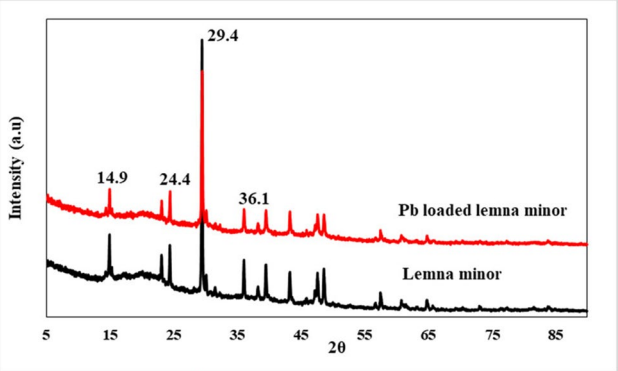

Fig. 2 XRD spectra in the absence and presence of Pb^{2+}

was characteristic of *L. minor* and could be considered to be occupied by Pb^{2+}.

3.1.3 TGA

A TGA curve demonstrating the percent weight loss in the range from 25 to 900 °C before and after Pb^{2+} biosorption of *L. minor* biosorbent was produced (Fig. 3). Thermal stability of *L. minor* has reportedly been low [38]. Around 100 °C, mass loss begins with the removal of free and bound water [38], causing the indicated thermal decomposition of hemicellulose and cellulose between 250 and 350 °C. Further elevations decompose the remaining cellulose and lignin [36]. The TGA curves of *L. minor* before and after biosorption were similar. However, a slight increase in thermal stability after biosorption might mean that biosorption process improved the thermal stability of *L. minor*.

3.1.4 SEM–EDX characterization

Morphological structure of *L. minor* before and after biosorption was presented (Fig. 4a, b). *L. minor* biomass displayed an irregular, heterogeneous surface with

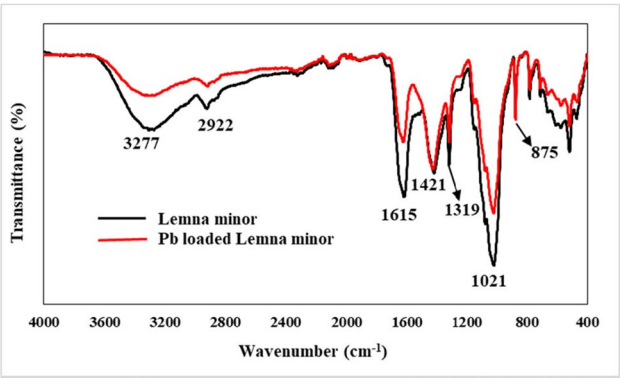

Fig. 1 FTIR spectra of *L. minor* and Pb^{2+}-loaded *L. minor*

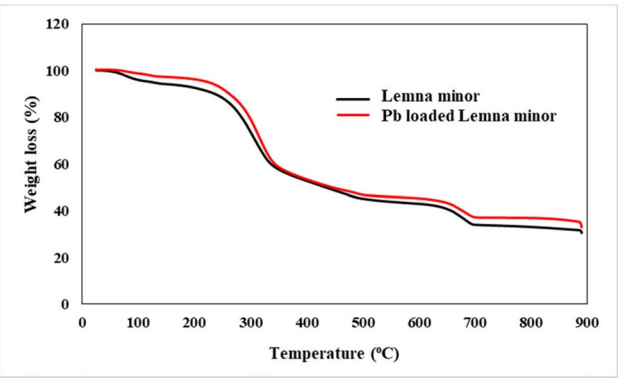

Fig. 3 TGA curves of empty and Pb^{2+}-loaded *L. minor*

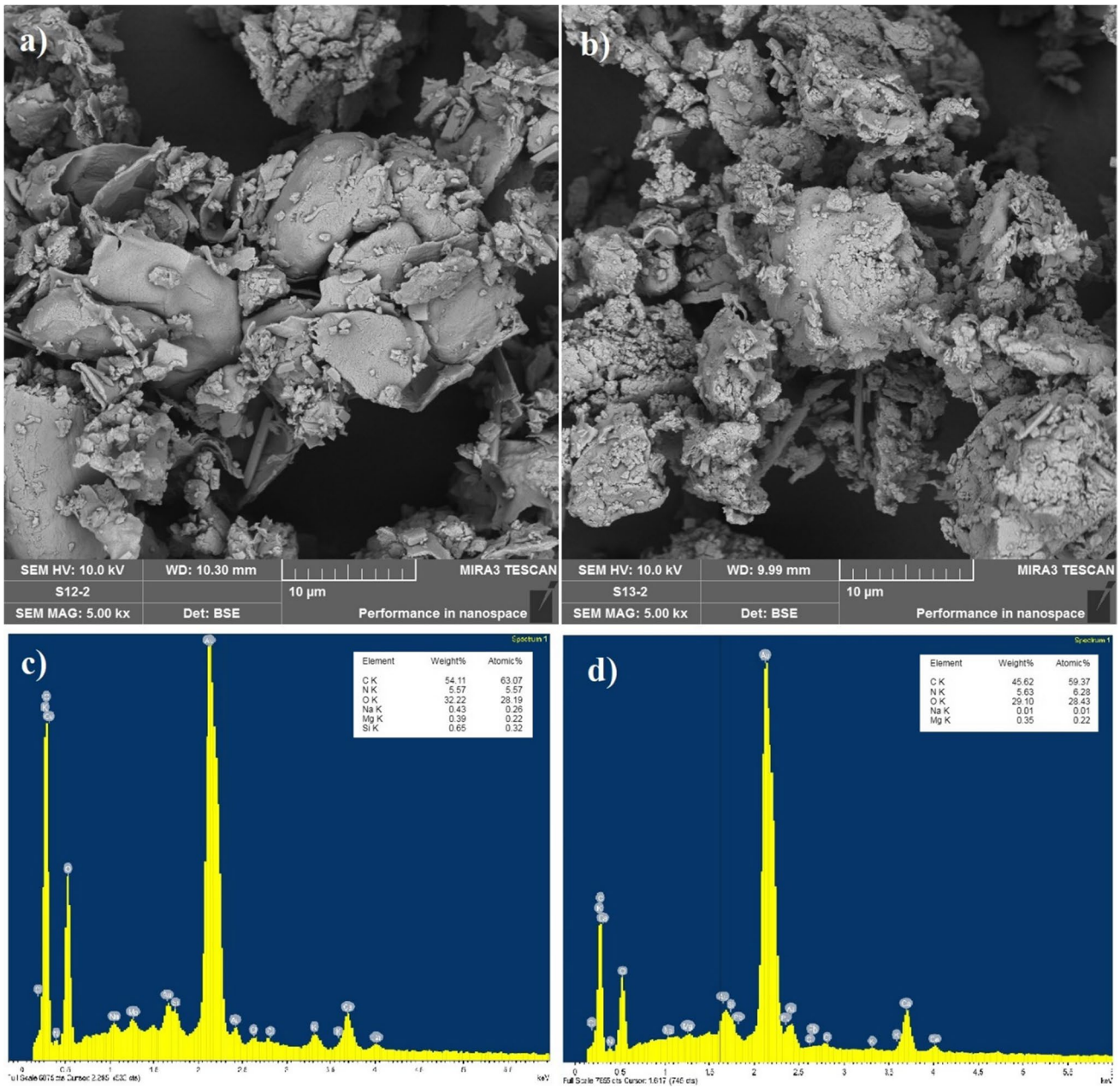

Fig. 4 SEM images for Pb^{2+} biosorption of *L. minor*: **a** before, **b** after; and EDX spectra for Pb biosorption of *L. minor*: **c** before, **d** after

differing particle sizes [38, 40]. This surface heterogeneity lessened and agglomerations appeared after biosorption [34]. EDX images and elemental analysis before and after biosorption indicated that *L. minor* possessed C and O densities (Fig. 4c, d). The C element density decreased after biosorption. This result may indicate that C-containing functional groups in the structure interacted with Pb^{2+} during biosorption. This notion gained further strength by FTIR spectra.

3.2 Effect of pH

The biosorption seemed to have highly influenced by the pH of the Pb^{2+} solution, possibly through charge interactions between the surface of sorbent and metal ion. The adsorption percentages versus pH were plotted at the acidic range (Fig. 5). Above this pH range, Pb^{2+} precipitated. A maximum adsorption was obtained at pH 4.5, and the remaining of the experiments was conducted at this pH. The effect of pH can be described by considering the point of zero charge

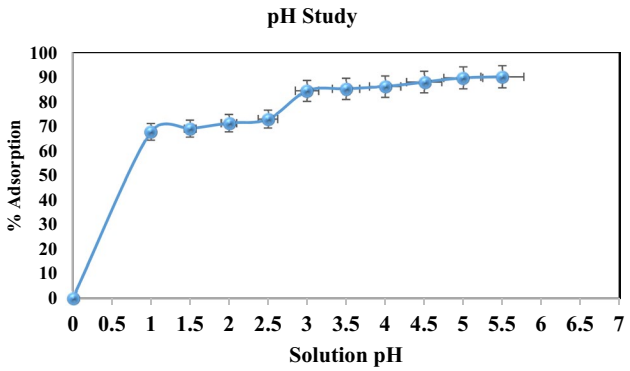

Fig. 5 Effect of pH on adsorption

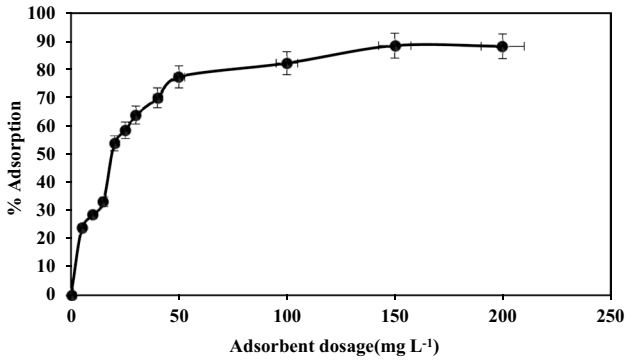

Fig. 6 Effect of adsorbent dosage on adsorption

of the biosorbent (pHpzc). The sorbent surface was positively charged below pH 3.2 and it negatively charged at pH value above 3.2. Therefore, for the pH values below 3.2, the adsorption was not favorable on account of the electrostatic repulsions between the Pb^{2+} and sorbent functional groups.

3.3 Effect of biosorbent amount

The adsorption percentage increased initially and then attained the equilibrium at 88.4% with the biosorbent dose of 150 mg L^{-1} (Fig. 6). Adsorption increased with increasing the biosorbent amount up to a certain point where further additions caused negligible increases, and increasing the adsorbent mass above 150 mg L^{-1} had no noticeable change in the adsorption percentage.

3.4 Adsorption isotherm models

The adsorption process was adjusted using different adsorption models. The adsorption models are helpful to describe the adsorbent and analyte interactions. The analysis of the adsorption isotherm data by different adsorption isotherm models is the main step to find the appropriate model which can be used for equilibrium study. Thus, to evaluate the fitness of the equilibrium outcomes, determination of R^2 coefficient, values of each model were analyzed. The Langmuir model envisions a homogenous monolayer adsorption at constant temperature (Eq. 1).

$$\frac{C_e}{C_{ads}} = \frac{1}{Qb} + \frac{C_e}{Q} \tag{1}$$

where Q is the monolayer adsorption capacity (mol g^{-1}); b is the adsorption enthalpy (mol L^{-1}); and C_e and C_{ads} are the equilibrium and adsorbed concentrations, respectively. The Langmuir model was applied to the equilibrium data, and a curve was produced by plotting the values of C_e versus Ce/C_{ads} (Fig. 7). The Langmuir capacity Q (mmol L^{-1}) and b (mol L^{-1}) were calculated from the slope and intercept (Table 1). $R^2 = 0.99$, obtained from this model, clearly demonstrated the suitability of the model. Furthermore, the Langmuir isotherms also indicated that the biosorbent surface had a good monolayer capacity which was identified by dimensionless constant separation factor (R_L) (Eq. 2).

$$R_L = \frac{1}{\left(1 + bC_i\right)} \tag{2}$$

where C_i is the initial Pb^{2+} concentration and R_L indicates whether adsorption is unfavorable: $R_L > 1$; linear: $R_L = 1$; favorable: $0 < R_L < 1$; irreversible: $R_L = 0$. Our R_L values resided between 0.34 and 0.89, indicating a favorable adsorption ($0 < R_L < 1$, Table 1 and Fig. 8).

The Freundlich isotherm model is suitable when the adsorbent surface is heterogeneous and the adsorption is multilayered. In this study, the logarithmic Freundlich formula was employed (Eq. 3).

$$\log C_{ads} = \log A + \left(\frac{1}{n}\right) \log C_e \tag{3}$$

where C_{ads} is the Freundlich equilibrium capacity; log (A) is the Freundlich adsorption constant; and n is the adsorption intensity. The graph was plotted between lnCads and lnCe, and the constant values were calculated from slope and intercept (Fig. 7). The n values ($n = 1.66$ and $1/n = 0.60$) suited best the Freundlich model (Table 1) because these values, between 1 and 10, indicated that the sorbent was heterogeneous and adsorption took place.

Dubinin–Radushkevich (D–R) isotherm estimates the mean free energy of sorption system (Eqs. 4–6).

$$\ln C_{ads} = \ln X_m - \beta\varepsilon^2 \tag{4}$$

$$\varepsilon = RT \ln\left(1 + \frac{1}{C_e}\right) \tag{5}$$

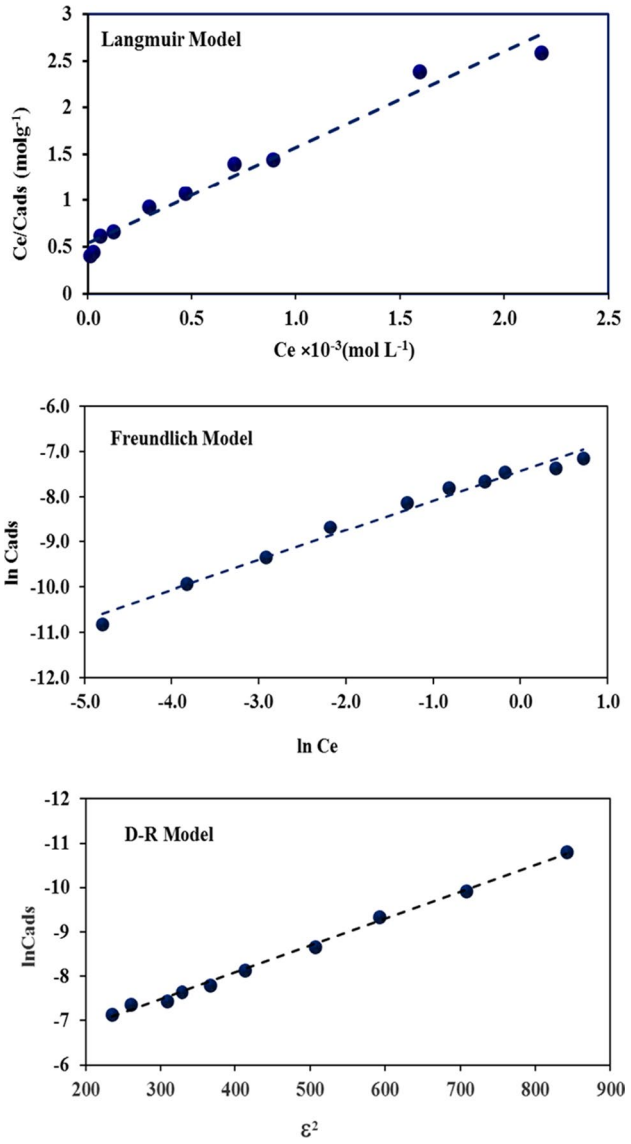

Fig. 7 The Langmuir, Freundlich, and D–R equilibrium models for the adsorption

Table 1 Adsorption constant values for the Langmuir, Freundlich, and D–R models

Parameters	Langmuir	Freundlich	D–R
Q (mmol g^{-1})	969.18	_	_
b	1.91	_	_
R_L	0.34–0.91	_	_
A (mmol g^{-1})	_	261.75	_
$1/n$	_	0.60	_
n	_	1.66	_
X_m (mmol g^{-1})	_	_	3.48
E (kJ mol^{-1})	_	_	9.05
R^2	0.986	0.980	0.99

$$E = \frac{1}{\sqrt{-2\beta}} \tag{6}$$

where ε is the Polanyi potential, X_m is the monolayer sorption capacity (mmol g^{-1}), and E is the mean energy (kJ mol^{-1}). The curve was obtained using lnCads against ε (Fig. 7). E (kJ mol^{-1}) values lied between 8 and 16 kJ mol^{-1}, indicating that biosorption involved a chemical reaction through ion-exchange events (Table 1).

3.5 Thermodynamic study

Thermodynamic studies helped us examine the temperature effect on the adsorption Pb^{2+}. The temperature effect on the biosorption of Pb^{2+} ion was experienced at 278, 298, and 313 K°. To understand whether the biosorption was endothermic or exothermic, $\Delta H°$, $\Delta S°$, and $\Delta G°$ were calculated using Eqs. 7 and 8.

$$\ln k_c = \frac{-\Delta H}{RT} + \frac{\Delta S}{R} \tag{7}$$

$$\Delta G = -RT \ln k_c \tag{8}$$

where k_c is the thermodynamic equilibrium constant, T is the absolute temperature (K°), and R is the gas constant. $\Delta H°$ and $\Delta S°$ were computed from the slope and intercept of linear plot of $ln\ k_c$ versus $1/T$ (Fig. 9) that described the pathway of Pb^{2+} ions sorption (Table 2). Negative ΔG pointed to a spontaneous and thermodynamically favorable adsorption, while the ΔS values suggested that the randomness increased at a given temperature at the solid biosorbent interface (Table 2).

3.6 Kinetic study

The biosorption rate constants for the sorption of Pb^{2+} were calculated using the pseudo-first-order (PFO) and pseudo-second-order (PSO) kinetic models. The PFO for Pb^{2+} ions sorption was calculated by using the Eq. 9.

$$\ln (q_e - q_t) = \ln q_e - k_1 t \tag{9}$$

where q_e is the mg mol^{-1} Pb^{2+} adsorbed per unit mass of biosorbent at equilibrium; q_t is the amount of Pb^{2+} adsorbed at a given t time; and k_1 is the rate constant of PFO kinetic model. The values of k_1 and q_e were calculated from slope and intercept of the linear plot of ln $(q_e - q_t)$ versus t (Fig. 10). The linear plot of ln $(q_e - q_t)$ versus t showed a poor correlation coefficient value (R^2, 0.77). The pseudo-second-order (PSO) rate equation was used to define the chemisorption concerning the valence forces by sharing/exchange of electrons between the sorbent and analyte (Eq. 10).

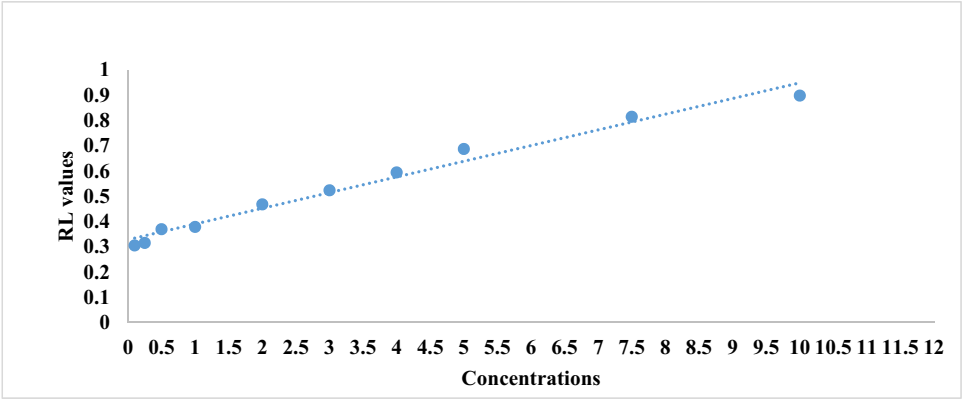

Fig. 8 R_L constant graph between initial concentration and R_L values

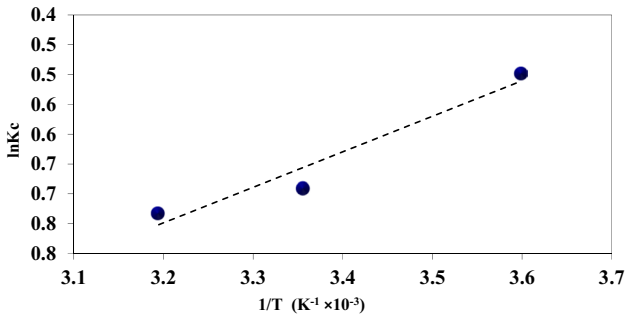

Fig. 9 Effect of temperature on the Pb^{2+} adsorption

Table 2 Thermodynamic parameters of Pb^{2+} adsorption

ΔH (kJ mol^{-1})	ΔS (kJ mol^{-1})	ΔG (kJ mol^{-1})		
		278 K	298 K	313 K
0.0049	0.0230	1.15	1.17	1.90
		$lnKc = 0.5$	$lnKc = 0.7$	$lnKc = 0.7$

$$\frac{t}{q_t} = \left(\frac{t}{k_2 q_e^2}\right) + \left(\frac{1}{q_e}\right) \tag{10}$$

where k_2 is the rate constant of PSO for the sorption of Pb^{2+}. The values of k_2 and q_e were calculated from the slope and intercept of the linear plots of t/q_t versus t (Fig. 10). The straight line with correlation coefficient values (R^2, 0.99) indicated the applicability of the PSO model (Table 3). By comparing the constant values of PFO and PSO, it became clear that the biosorption fitted the PSO model.

3.7 Computational study

As hemicellulose, galactoglucomannan (GGM), the commonest softwood hemicellulose, was used. Similarly, a lignin polymer, made up of ether bonded coniferyl alcohol residues, was chosen. In addition, galacturonic acid (GA) was preferred as the main component of pectin (Figs. 11, 12, and 13). The ion-containing GA/Pb^{2+} complex was envisaged as a singlet and a triplet, while the other lignin/Pb^{2+} and GGM/Pb^{2+} complexes were analyzed as triplets (Table 4). The adsorption energy was determined as follows (Eq. 11):

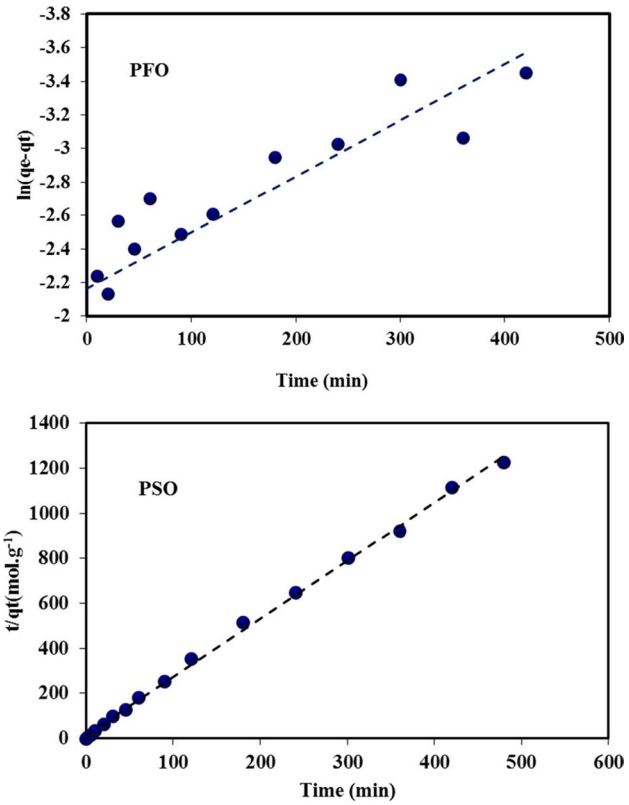

Fig. 10 PFO and PSO kinetic models for Pb^{2+} adsorption

$$E_{ads} = E(\text{molecule}) + E\left(Pb^{2+}\right) - E\left(\text{molecule}/Pb^{2+}\right) \tag{11}$$

It should be noted that, for all the considered complexes, the lead ion tended to form strong covalent bonds with oxygen atoms (Figs. 14, 15, 16, and 17).

Table 3 Pseudo-first- and second-order constant values for the adsorption of Pb^{2+}

Pseudo-first-order				Pseudo-second-order		
Pb^{2+}	K_1 (min^{-1})	q_e (mmol g^{-1})	R^2	K_2 (min^{-1})	q_e (mmol g^{-1} min^{-1})	R^2
	2.86	996	0.830	0.382	150.45	0.998

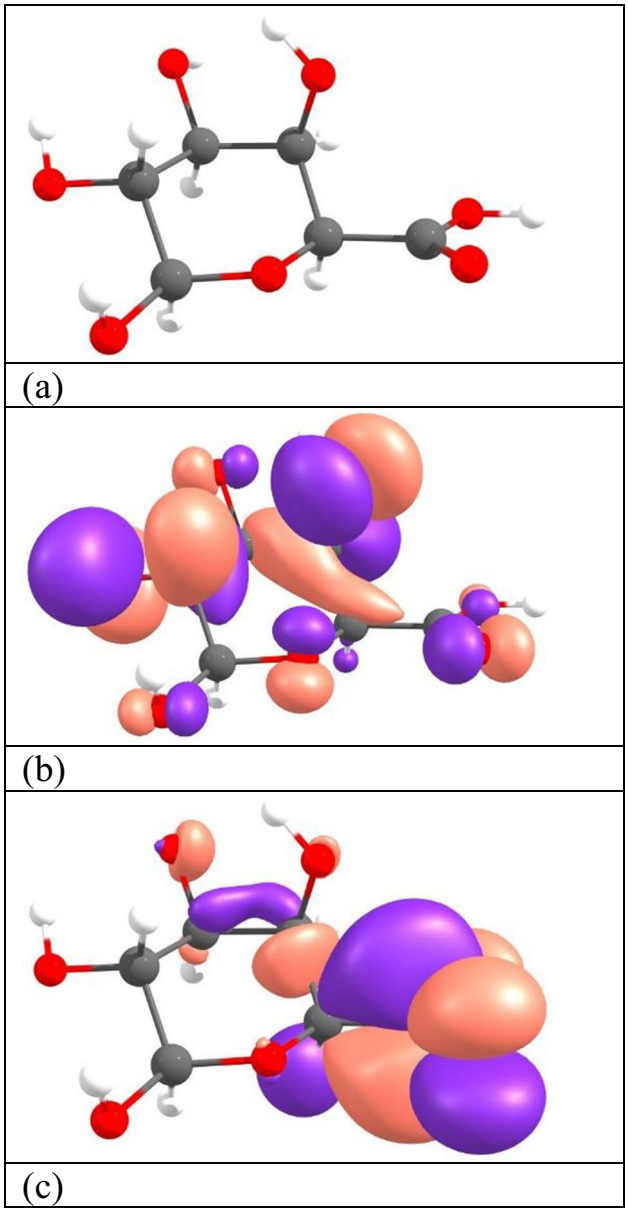

Fig. 11 GA: atomic structure (**a**), HOMO (**b**), and LUMO (**c**) [28–31]

The interactions of the dominant species in the studied plant extract with Pb^{2+} were also examined theoretically. For this aim, important quantum chemical parameters were calculated and presented in Table 4. According to Koopmans' theorem [41], ground state ionization energy and electron affinity of any molecular system can be calculated from frontier orbital energies as [42]:

$$I = -E_{\mathrm{HOMO}} \tag{12}$$

$$A = -E_{\mathrm{LUMO}} \tag{13}$$

In conceptual DFT, chemical hardness (η) is calculated as [43]:

$$\eta = I - A \tag{14}$$

$$\eta = E_{\mathrm{LUMO}} - E_{\mathrm{HOMO}} \tag{15}$$

Chemical hardness is reported as the resistance against electron cloud polarization of chemical systems. First electronic structure principle about chemical hardness concept is hard and soft acid–base (HSAB) principle [44]. According to HSAB principle, "hard acids prefer the binding to hard bases and soft acids prefer the binding o soft bases." Softness (σ) is given the inverse of the hardness as $\sigma = 1/\eta$. Second electronic structure principle about the hardness is maximum hardness principle stating that "It seems to be a rule of nature that molecules arrange themselves so as to be as hard as possible" [45]. In HSAB classification, Pb^{2+} is among soft acids. For that reason, this ion interacts more powerful with the molecules of low chemical hardness (Table 4). Calculated adsorption energies and chemical hardness values are in good agreement and our data supports the HSAB principle.

4 Comparative study

The *Lemna minor* biosorbent has been compared with previously used sorbent for the removal of metal ions. Table 5 shows that the biosorbent has comparable adsorption efficiency with other reported adsorbents.

5 Conclusion

Lemna minor powder displayed an excellent potential for Pb^{2+} sorption in aqueous media and a maximum sorption could be possible at pH 4.5. Experimental findings fitted best the Langmuir model (R^2, 0.98; 969.18 mmol g^{-1}). Thermodynamic parameters indicated that the biosorption of Pb^{2+} was spontaneous and endothermic. The kinetic suited better to PSO model, confirming that chemisorption took place.

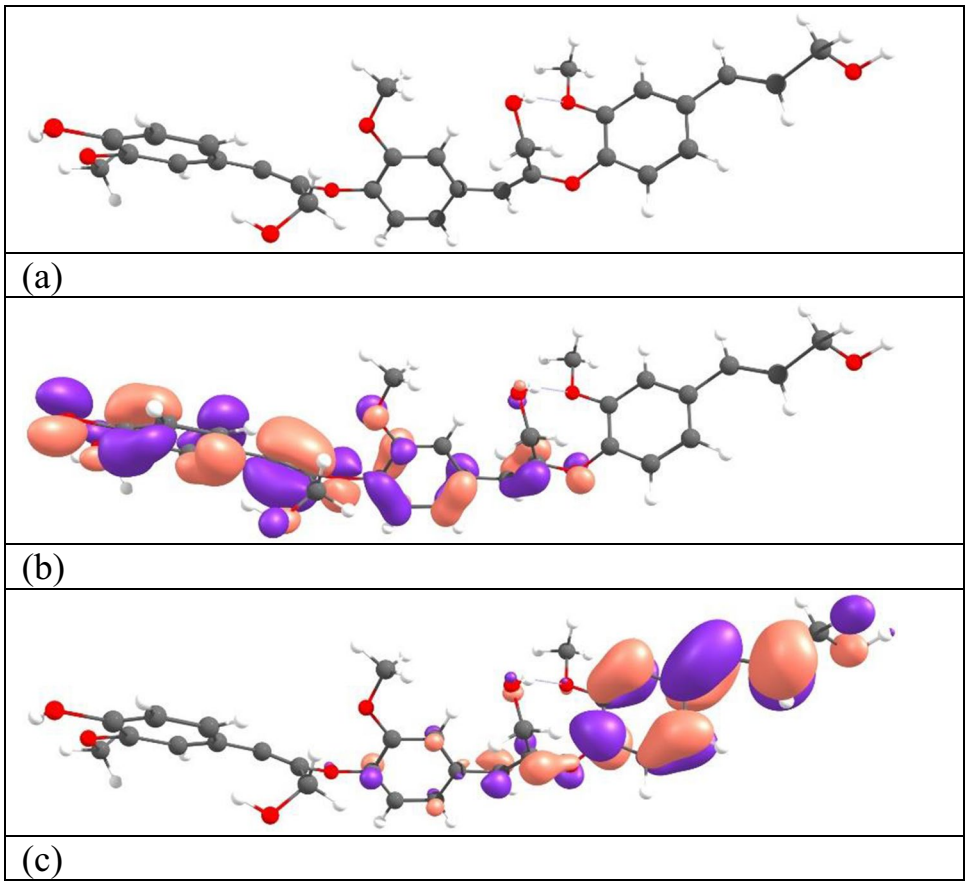

Fig. 12 Lignin: atomic structure (**a**), HOMO (**b**), and LUMO (**c**) [28–31]

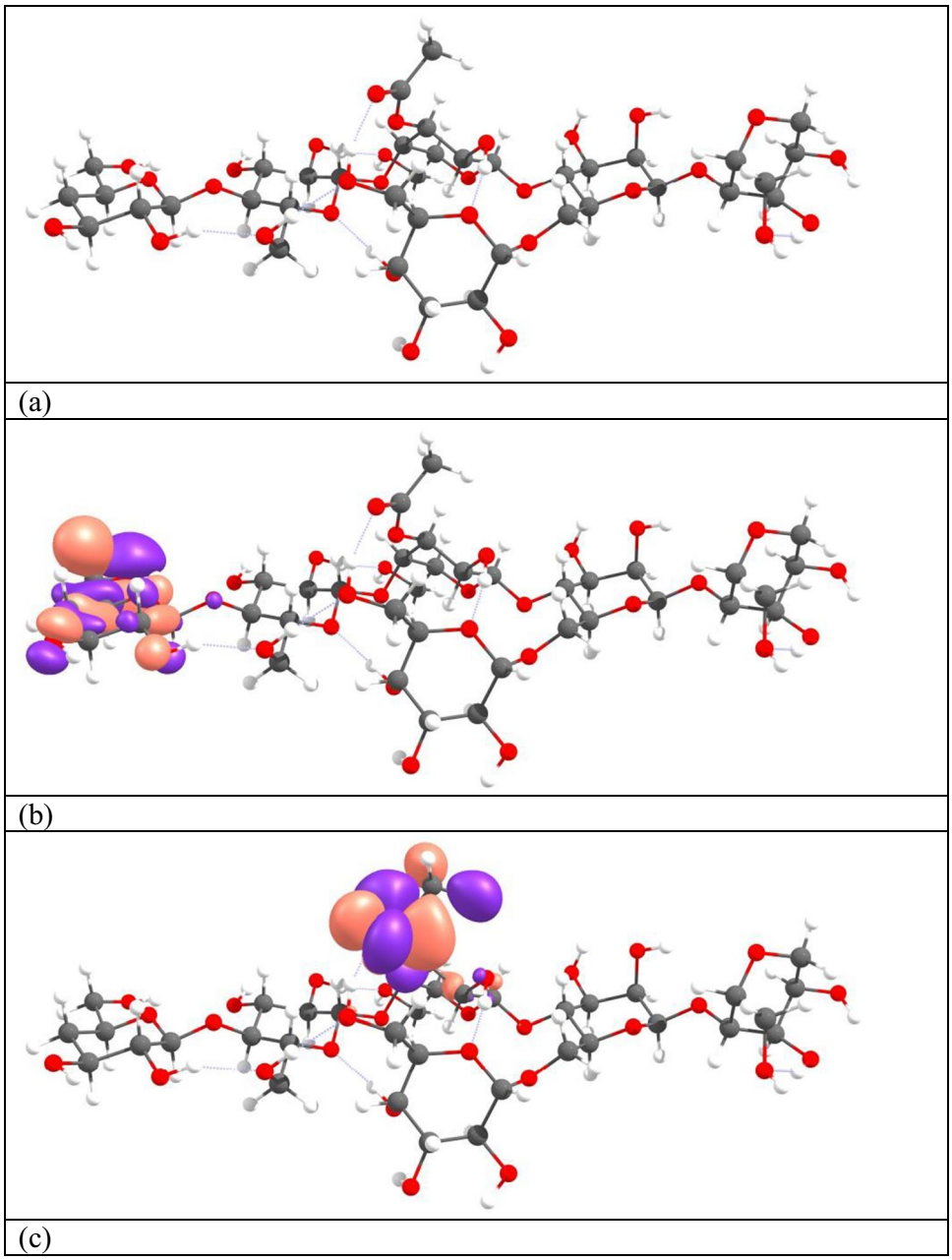

Fig. 13 GGM: atomic structure (**a**), HOMO (**b**), and LUMO (**c**) [28–31]

Table 4 Calculated electronic characteristics of unsubstituted GGM, lignin, GA, and their complexes with Pb^{2+}

Name	Dipole moment (Debye)	HOMO (eV)	LUMO (eV)	Gap (eV)	E_{ads} (eV)
GA	5.331	− 5.910	− 0.868	5.042	-
Lignin	5.557	− 4.280	− 2.057	2.223	-
GGM	8.794	− 5.298	− 1.760	3.538	-
GA/Pb^{2+} (S)	5.746	− 13.268	− 10.934	2.335	7.76
GA/Pb^{2+} (T)	15.514	− 10.003	− 9.690	0.313	14.72
Lignin/Pb^{2+}	3.709	− 8.479	− 7.869	0.610	18.16
GGM/Pb^{2+}	6.001	− 7.973	− 7.497	0.476	18.20

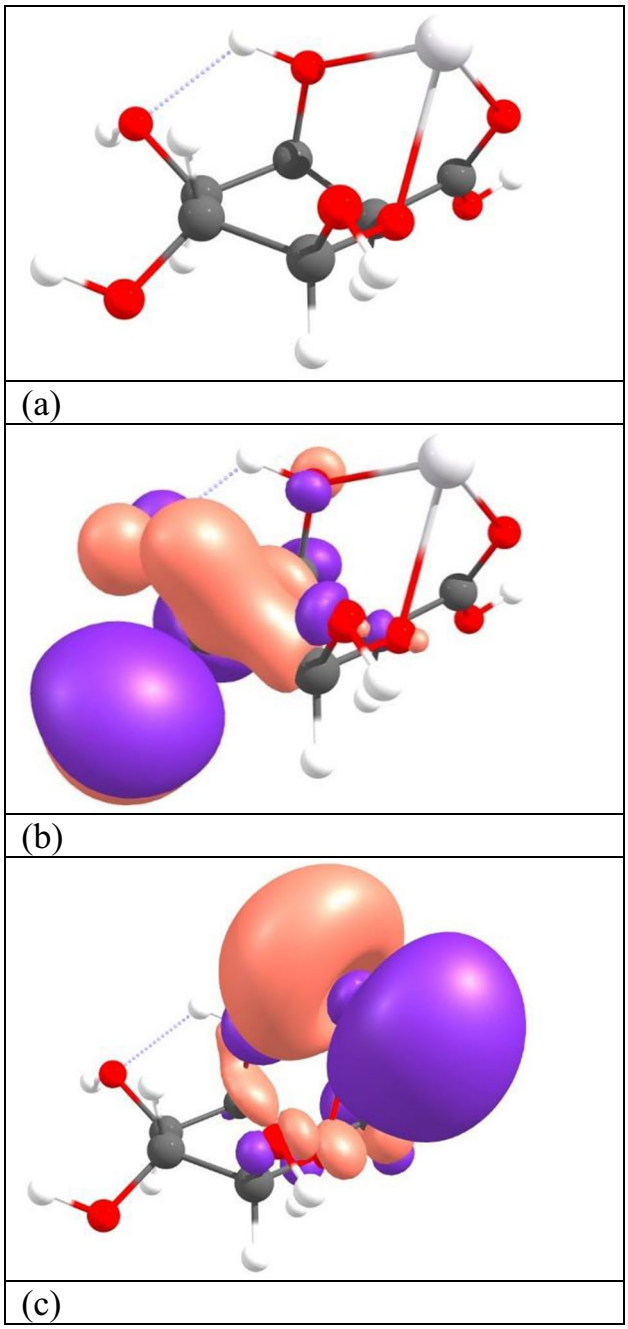

Fig. 14 GA/Pb.$^{2+}$ (S): atomic structure (**a**), HOMO (**b**), and LUMO (**c**)

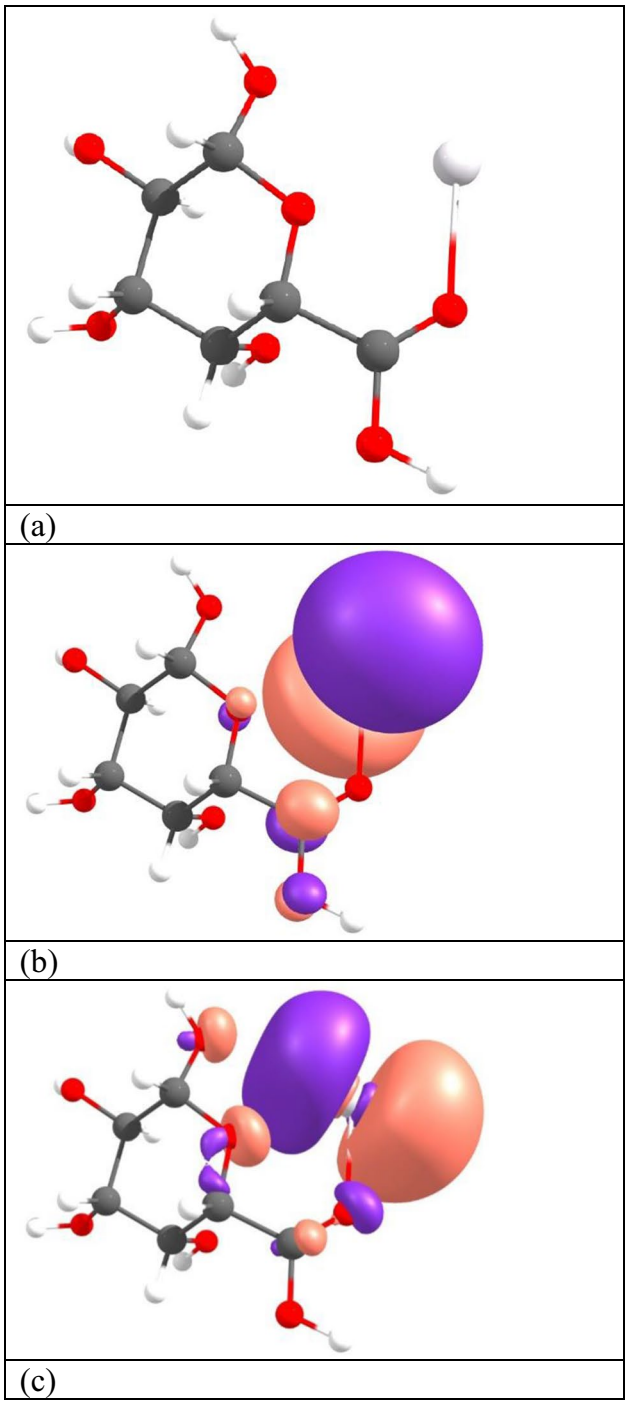

Fig. 15 GA/Pb.$^{2+}$ (T): atomic structure (**a**), HOMO (**b**), and LUMO (**c**)

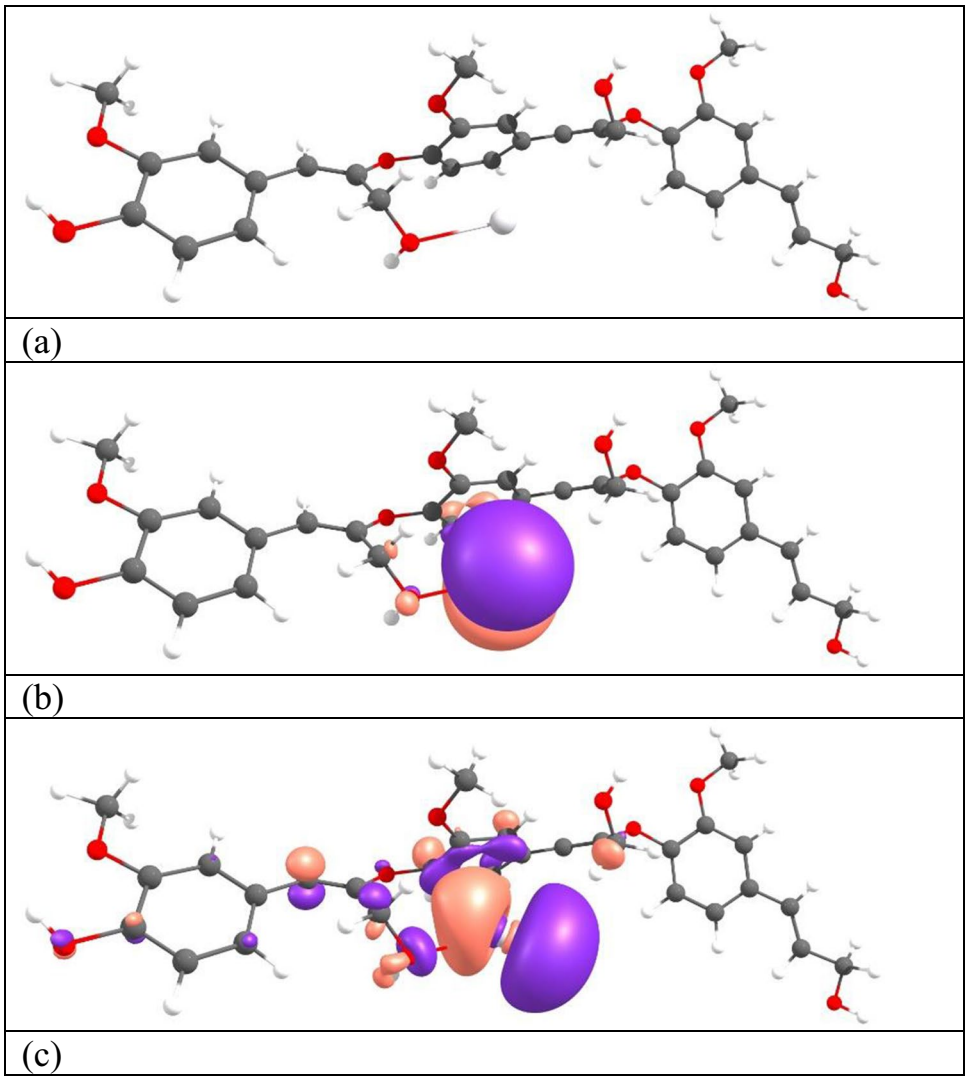

Fig. 16 Lignin/$Pb.^{2+}$: atomic structure (**a**), HOMO (**b**), and LUMO (**c**)

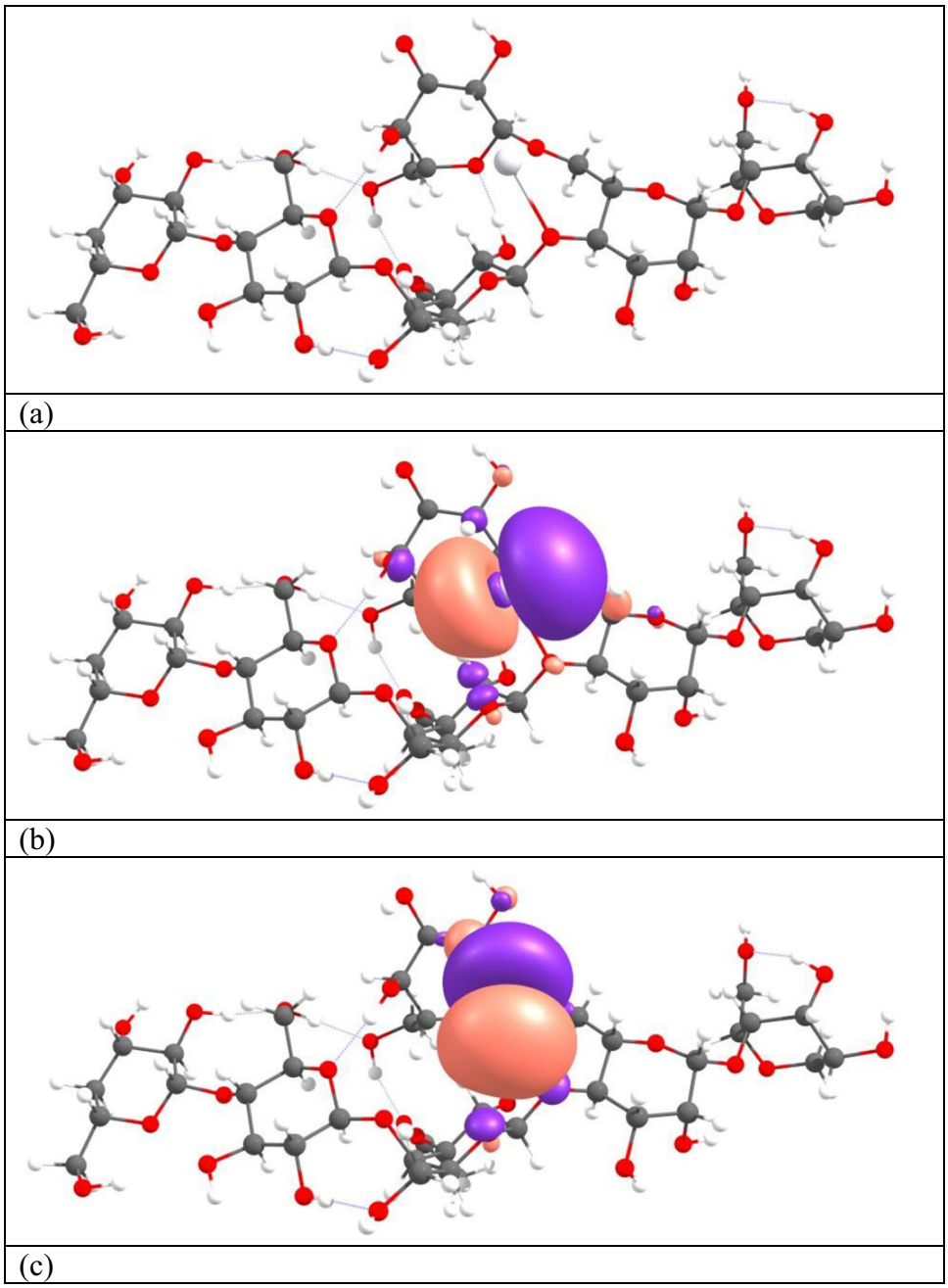

Fig. 17 GGM/$Pb.^{2+}$: atomic structure (**a**), HOMO (**b**), and LUMO (**c**)

Table 5 Comparison of functionalized silica resin with reported adsorbent

Adsorbent	Metal ions	Sorption capacities	References
Banana peel	Cd^{2+} ions and Pb^{2+} ions	93.2 and 83.78%, respectively	[46]
Rice husk ash	Pb^{2+} ions	75%	[47]
Bagasse biochar	Pb^{2+} ions	75.4%	[48]
Lemna minor	Pb^{2+} ions	769.23 mg g^{-1}	Current study

Author contribution Savaş Kaya: conceptualization, methodology, supervision, writing—original draft.

Serap Çetinkaya: data curation, investigation, writing—review and editing.

Nida Shams Jalbani: investigation, validation.

Ali Fazıl Yenidünya: resources, investigation, writing—review and editing.

Nurşah Kütük: writing—review and editing.

Ergün Kasaka: methodology, writing—original draft.

Mikhail M. Maslov: writing—review and editing.

Data availability All the data that support the results of this research are available within the manuscript.

Declarations

Ethical approval Not applicable.

Competing interests The authors declare no competing interests.

References

1. Kamal B, Rafey A (2021) A mini review of treatment methods for lead removal from wastewater. Int J Environ Anal Chem 1–16. https://doi.org/10.1080/03067319.2021.1934833
2. Saravanan A, Kumar PS, Jeevanantham S, Karishma S, Tajsabreen B, Yaashikaa PR, Reshma B (2021) Effective water/wastewater treatment methodologies for toxic pollutants removal: processes and applications towards sustainable development. Chemosphere 280:130595. https://doi.org/10.1016/j.chemosphere.2021.130595
3. Bharti R, Sharma R (2022) Effect of heavy metals: an overview. Mater Today Proc 51:880–885. https://doi.org/10.1016/j.matpr.2021.06.278
4. Briffa J, Sinagra E, Blundell R (2020) Heavy metal pollution in the environment and their toxicological effects on humans. Heliyon 6:e04691. https://doi.org/10.1016/j.heliyon.2020.e04691
5. Rosen MB, Pokhrel LR, Weir MH (2017) A discussion about public health, lead and Legionella pneumophila in drinking water supplies in the United States. Sci Total Environ 590–591:843–852. https://doi.org/10.1016/j.scitotenv.2017.02.164
6. Cimá-Mukul CA, Olguín MT, Abatal M, Vargas J, Barrón-Zambrano JA, Avila-Ortega A, Santiago AA (2020) Assessment of Leucaena leucocephala as bio-based adsorbent for the removal of pb^{2+}, cd^{2+} and ni^{2+} from water. Desalin Water Treat 173:331–342. https://doi.org/10.5004/dwt.2020.24736
7. El-Amier YA, Elsayed A, El-Esawi MA, Noureldeen A, Darwish H, Fakhry H (2021) Optimizing the biosorption behavior of Ludwigia stolonifera in the removal of lead and chromium metal ions from synthetic wastewater. Sustainability 13:6390. https://doi.org/10.3390/su13116390
8. Issayeva A, Myrzabayeva Z, Kidirbayeva K, Ibragimov T, Baitasheva G, Tleukeyeva A (2022) Reaction of aquatic plants of small rivers of the Turkestan region of Kazakhstan to heavy metal ions. Ecol Eng 23:43–49. https://doi.org/10.12911/22998993/147838
9. Lima LKS, Kleinübing SJ, Silva EA, Silva MGC (2011) Removal of chromium from wastewater using macrophytes Lemna Minor as biosorbent. Chem Eng Trans 25:303–308
10. Lesmana OS, Febriana N, Soetaredjo EF, Ismadji S (2009) Studies on potential applications of biomass for the separation of heavy metals from water and wastewater. Biochem Eng J 44:19–41. https://doi.org/10.1016/j.bej.2008.12.009
11. Priyadarshanee M, Das S (2021) Biosorption and removal of toxic heavy metals by metal tolerating bacteria for bioremediation of metal contamination: a comprehensive review. Environ. Chem. Eng 9:104686. https://doi.org/10.1016/j.jece.2020.104686
12. Ayele A, Godeto YG (2021) Bioremediation of chromium by microorganisms and its mechanisms related to functional groups. J Chem 2021:1–21. https://doi.org/10.1155/2021/7694157
13. Fouda-Mbanga BG, Prabakaran E, Pillay K (2021) Carbohydrate biopolymers, lignin based adsorbents for removal of heavy metals (Cd^{2+}, Pb^{2+}, Zn^{2+}) from wastewater, regeneration and reuse for spent adsorbents including latent fingerprint detection: a review. Biotechnol Rep 30:e00609. https://doi.org/10.1016/j.btre.2021.e00609
14 Dammak M, Hlima HB, Tounsi L, Michaud P, Fendri I, Abdelkafi S (2022) Effect of heavy metals mixture on the growth and physiology of Tetraselmis sp.: applications to lipid production and bioremediation. Bioresour Technol 360:127584. https://doi.org/10.1016/j.biortech.2022.127584
15. Zhao X, Moates GK, Wellner N, Collins SRA, Coleman MJ, Waldron KW (2014) Chemical characterisation and analysis of the cell wall polysaccharides of duckweed (Lemna minor). Carbohydr Polym 111:410–418. https://doi.org/10.1016/j.carbpol.2014.04.079
16. Khan MA, Wani GA, Majid H, Farooq FU, Reshi ZA, Husaini AM, Shah MA (2020) Differential bioaccumulation of select heavy metals from wastewater by *Lemna minor*. Bull Environ Contam Toxicol 105:777–783. https://doi.org/10.1007/s00128-020-03016-3
17. Ekperusi AO, Sikoki FD, Nwachukwu EO (2019) Application of common duckweed (Lemna minor) in phytoremediation of chemicals in the environment: state and future perspective. Chemosphere 223:285–309. https://doi.org/10.1016/j.chemosphere.2019.02.025
18. Balasubramanian UM, Vaiyazhipalayam Murugaiyan S, Marimuthu T (2020) Enhanced adsorption of Cr (VI), Ni (II) ions from aqueous solution using modified Eichhornia crassipes and Lemna minor. Environ Sci Pollut Res 27:20648–20662. https://doi.org/10.1007/s11356-019-06357-7
19. Hurd NA, Sternberg SPK (2008) Bioremoval of aqueous lead using Lemna minor. Int J Phytoremediation 10:278–288. https://doi.org/10.1080/15226510802096036
20. Ifthikar J, Jiao X, Ngambia A, Wang T, Khan A, Jawad A, Xue Q, Liu L, Chen Z (2018) Facile one-pot synthesis of sustainable carboxymethyl chitosan - sewage sludge biochar for effective heavy metal chelation and regeneration. Bioresour Technol 262:S0960852418305662. https://doi.org/10.1016/j.biortech.2018.04.053
21. Wang Q, Wang B, Lee X, Lehmann J, Gao B (2018) Sorption and desorption of Pb(II) to biochar as affected by oxidation and pH. Sci Total Environ 634:188–194. https://doi.org/10.1016/j.scitotenv.2018.03.189
22. Wu W, Li J, Lan T, Müller K, Niazi NK, Chen X, Xu S, Zheng L, Chu Y, Li J (2017) Unraveling sorption of lead in aqueous solutions by chemically modified biochar derived from coconut fiber: a microscopic and spectroscopic investigation. Sci Total Environ 576:766–774. https://doi.org/10.1016/j.scitotenv.2016.10.163
23. Yan FL, Wang Y, Wang WH, Zhao JX, Feng LL, Li JJ, Zhao JC (2020) Application of biochars obtained through the pyrolysis of Lemna minor in the treatment of Ni-electroplating wastewater. J Water Process Eng 37:101464. https://doi.org/10.1016/j.jwpe.2020.101464
24. Baybaş D, Ulusoy U (2011) Polyacrylamide–clinoptilolite/Y-zeolite composites: characterization and adsorptive features for terbium. J Hazard Mater 187:241–249. https://doi.org/10.1016/j.jhazmat.2011.01.014
25. Perdew JP, Burke K, Ernzerhof M (1996) Generalized gradient approximation made simple. Phys Rev Lett 77:3865–3868. https://doi.org/10.1103/PhysRevLett.77.3865

26. Weigend F, Ahlrichs R (2005) Balanced basis sets of split valence, triple zeta valence and quadruple zeta valence quality for H to Rn: design and assessment of accuracy. Phys Chem Chem Phys 7:3297–3305. https://doi.org/10.1039/B508541A
27. Grimme S, Antony J, Ehrlich S, Krieg H (2010) A consistent and accurate *ab initio* parametrization of density functional dispersion correction (DFT-D) for the 94 elements H-Pu. J Chem Phys 132:154104. https://doi.org/10.1063/1.3382344
28 Ufimtsev IS, Martínez TJ (2009) Quantum chemistry on graphical processing units. 3. Analytical energy gradients and first principles molecular dynamics. J Chem Theo Comp 5:2619. https://doi.org/10.1021/ct9003004
29. Titov AV, Ufimtsev IS, Luehr N, Martínez TJ (2013) Generating efficient quantum chemistry codes for novel architectures. J Chem Theo Comp 9:213. https://doi.org/10.1021/ct300321a
30. Kästner J, Carr JM, Keal TW, Thiel W, Wander A, Sherwood P (2009) DL-FIND: an open-source geometry optimizer for atomistic simulations. J Phys Chem A 113:11856. https://doi.org/10.1021/jp9028968
31. Goumans TPM, Catlow CRA, Brown WA, Kästner J, Sherwood P (2009) An embedded cluster study of the formation of water on interstellar dust grains. Phys Chem Chem Phys 11:5431. https://doi.org/10.1039/B816905E
32. Wang LP, Song C (2016) Geometry optimization made simple with translation and rotation coordinates. J Chem Phys 144:214108. https://doi.org/10.1063/1.4952956
33. Çetinkaya HF, Cebeci MS, Kaya S, Jalbani NS, Maslov MM, Marzouki E (2022) Removal of erythrosine B dye from wastewater using chitosan boric acid composite material: experimental and density functional theory findings. J Phys Org Chem e4400. https://doi.org/10.1002/poc.4400
34. Can-Terzi B, Goren AY, Okten HE, Sofuoglu SC (2021) Biosorption of methylene blue from water by live Lemna minor. Environ Technol Innov 22:101432. https://doi.org/10.1016/j.eti.2021.101432
35. Saygideger S, Gulnaz O, Istifli ES, Yucel N (2005) Adsorption of Cd (II), Cu (II) and Ni (II) ions by Lemna minor L.: effect of physicochemical environment. J Hazard Mater 126:96–104. https://doi.org/10.1016/j.jhazmat.2005.06.012
36. Romero-Guzmán ET, Reyes-Gutiérrez LR, Marín-Allende MJ, González-Acevedo ZI, Olguín-Gutiérrez MT (2013) Physicochemical properties of non-living water hyacinth (Eichhornia crassipes) and lesser duckweed (Lemna minor) and their influence on the As (V) adsorption processes. Chem Ecol 29:459–475. https://doi.org/10.1080/02757540.2013.772589
37. Imron MF, Ananta AR, Ramadhani IS, Kurniawan SB, Abdullah SRS (2021) Potential of Lemna minor for removal of methylene blue in aqueous solution: kinetics, adsorption mechanism, and degradation pathway. Environ Technol Innov 24:101921. https://doi.org/10.1016/j.eti.2021.101921
38. Yoksan R, Boontanimitr A, Klompong N, Phothongsurakun T (2022) Poly (lactic acid)/thermoplastic cassava starch blends filled with duckweed biomass. Int J Biol Macromol 203:369–378. https://doi.org/10.1016/j.ijbiomac.2022.01.159
39. Nassar HF, Ibrahim M (2021) Duckweed-Lemna minor as green route for removal of chromium (VI) from aqueous solution. Int J Environ Res 15:275–284. https://doi.org/10.1007/s41742-021-00314-4
40. Balarak D, Pirdadeh F, Mahdavi Y (2015) Biosorption of Acid Red 88 dyes using dried Lemna minor biomass. J Sci Technol Environ 1:81–90
41. Koopmans T (1934) Über die Zuordnung von Wellenfunktionen und Eigenwerten zu den einzelnen Elektronen eines Atoms. Physica 1(1–6):104–113. https://doi.org/10.1016/S0031-8914(34)90011-2
42. Kaya S, Kaya C (2015) A new equation for calculation of chemical hardness of groups and molecules. Mol Phys 113(11):1311–1319. https://doi.org/10.1080/00268976.2014.991771
43 Islam N, Kaya S (eds) (2018) Conceptual density functional theory and its application in the chemical domain. CRC Press
44. Pearson RG (1963) Hard and soft acids and bases. J Am Chem Soc 85(22):3533–3539
45. Kaya S, Kaya C (2015) A simple method for the calculation of lattice energies of inorganic ionic crystals based on the chemical hardness. Inorg Chem 54(17):8207–8213. https://doi.org/10.1021/acs.inorgchem.5b00383
46. Motaghi M, Ziarati P (2016) Adsorptive removal of cadmium and lead from Oryza sativa rice by banana peel as bio-sorbent. Biomed Pharmacol J 9(2):739–749. https://doi.org/10.13005/bpj/998
47. Nnaji CC, Ebeagwu CJ, Ugwu EI (2017) Physicochemical conditions for adsorption of lead from water by rice husk ash. BioResources 12(1):799–818
48. Bharti SK, Kumar N (2018) Kinetic study of lead (Pb^{2+}) removal from battery manufacturing wastewater using bagasse biochar as biosorbent. Appl Water Sci 8(4):1–13. https://doi.org/10.1007/s13201-018-0765-z